Chemical Vapor Deposition of Cerium Oxide Films from a Cerium Alkoxide Precursor

Seigi Suh, Jun Guan, Liliana A. Mîinea, Jean-Sébastien M. Lehn, and David M. Hoffman*

Department of Chemistry and Center for Materials Chemistry, University of Houston, Houston, Texas 77204-5003

Received December 31, 2003. Revised Manuscript Received February 17, 2004

The cerium(IV) alkoxide complex $Ce(OCMe_2\text{-}i\text{-}Pr)_4$, a volatile, nonfluorinated source of cerium, was used as a chemical vapor deposition precursor to cerium oxide films. A conventional thermal chemical vapor deposition process deposited cerium(IV) oxide films from $Ce(OCMe_2\text{-}i\text{-}Pr)_4$ on silicon, glass, quartz, lanthanum aluminum oxide (001), and roll-textured nickel (001) substrates at low substrate temperatures (<550 °C). The films were highly oriented when the depositions were carried out on lanthanum aluminum oxide and textured nickel substrates. An X-ray crystallographic study of $Ce(OCMe_2\text{-}i\text{-}Pr)_4$, which melts at just below room temperature, shows that it is a loosely bound dimer in the solid state with five-coordinate cerium centers and two bridging alkoxide ligands. The synthesis and X-ray crystal structures of $Ce(OCMe_2\text{-}i\text{-}Pr)_4(DMAP)_2$ (DMAP = 4-(dimethylamino)pyridine) and $Ce_2(OCMe_2\text{-}i\text{-}Pr)_5(acac)_3$ are also reported. The cerium atoms in $Ce(OCMe_2\text{-}i\text{-}Pr)_4(DMAP)_2$ and $Ce_2(OCMe_2\text{-}i\text{-}Pr)_5(acac)_3$ have, respectively, distorted octahedral and pentagonal bipyramidal coordination geometries.

Introduction

Current research on high-temperature superconductors is focused on the development of low-cost, high-throughput processes to prepare YBCO-based coated conductors.[1] A critical component in the manufacture of practical coated conductors will be the process used to deposit the buffer layer. The buffer layer provides a template for the deposition of YBCO and acts as a diffusion barrier between the substrate, such as nickel ribbon, and YBCO coating. One of the most studied and promising buffer layers for nickel/YBCO-coated conductor applications is cerium oxide.

In this paper we describe the preparation of cerium oxide films by chemical vapor deposition (CVD) using the homoleptic cerium alkoxide complex $Ce(OCMe_2\text{-}i\text{-}Pr)_4$ as the precursor. We also report the synthesis and crystal structures of $Ce(OCMe_2\text{-}i\text{-}Pr)_4(DMAP)_2$ (DMAP = 4-(dimethylamino)pyridine) and $Ce_2(OCMe_2\text{-}i\text{-}Pr)_5(acac)_3$, and the crystal structure of the parent compound $Ce(OCMe_2\text{-}i\text{-}Pr)_4$. Previous studies on the CVD of cerium oxide films have used primarily β-diketonate complexes (e.g., Ce[*t*-BuC(O)CHC(O)-*t*-Bu]$_4$), derivatives of β-diketonate complexes (e.g., $Ce[(CF_3C(O)CHC(O)CF_3)]_3(MeOCH_2CH_2OMe)$, and complexes with ligands that are closely related to β-diketonates as precursors.[2−18] There is one previous report on the attempted use of cerium alkoxide complexes as CVD precursors. In that study, Hubert-Pfalzgraf et al. produced as-deposited films containing a mixture of ceria and cerium(III) fluoride from the fluorinated alkoxide compounds $Ce[OCH(CF_3)_2]_4(Me_2NCH_2CH_2NMe_2)$ and $Ce[OCH(CF_3)_2]_4[Me(OCH_2CH_2)_2OMe)$.[19]

Experimental Section

Synthesis. Standard glovebox and Schlenk procedures were followed in the syntheses. Dry degassed solvents were used.

* To whom correspondence should be addressed. E-mail: hoffman@uh.edu.

(1) Izumi, T.; Yamada, Y.; Shiohara, Y. *Physica C* **2003**, *392−396* (Part 1), 9. Akin, Y. Aslanoglu, Z.; Celik, E.; Arda, L.; Sigmund, W.; Hascicek, Y. S. *IEEE Trans. Appl. Supercond.* **2003**, *13*, 2673.

(2) Edleman, N. L.; Wang, A.; Belot, J. A.; Metz, A. W.; Babcock, J. R.; Kawaoka, A. M.; Ni, J.; Metz, M. V.; Flaschenriem, C. J.; Stern, C. L.; Liable-Sands, L. M.; Rheingold, A. L.; Markworth, P. R.; Chang, R. P. H.; Chudzik, M. P.; Kannewurf, C. R.; Marks, T. J. *Inorg. Chem.* **2002**, *41*, 5005.

(3) Pollard, K. D.; Jenkins, H. A.; Puddephatt, R. J. *Chem. Mater.* **2000**, *12*, 701.

(4) McAleese, J.; Plakatouras, J. C.; Steele, B. C. H. *Thin Solid Films* **1996**, *280*, 152.

(5) Becht, M.; Morishita, T. *Chem. Vap. Deposition* **1996**, *2*, 191.

(6) Becht, M.; Gerfin, T.; Dahmen, K.-H. *Chem. Mater.* **1993**, *5*, 137.

(7) Dahmen, K.-H.; Becht, M.; Gerfin, T. *High T_c Supercond. Thin Films* **1992**, 715.

(8) Gerfin, T.; Becht, M.; Dahmen, K.-H. *Ber. Bunsen-Ges. Phys. Chem.* **1991**, *95*, 1564.

(9) Lu, Z.; Hiskes, R.; DiCarolis, S. A.; Nel, A.; Route, R. K.; Feigelson, R. S. *J. Cryst. Growth* **1995**, *156*, 227.

(10) Lo Nigro, R.; Malandrino, G.; Fragalà, I. L. *Chem. Mater.* **2001**, *13*, 4402.

(11) Lee, H.-G.; Lee, Y.-M.; Shin, H.-S.; Kim, C.-J. Hong, G.-W. *Mater. Sci. Eng.* **2002**, *B90*, 20.

(12) Liang, S.; Chern, C. S.; Shi, Z. Q.; Lu, P.; Lu, Y.; Kear, B. H. *J. Cryst. Growth* **1995**, *151*, 359.

(13) Ignatiev, A.; Chou, P. C.; Zhong, Q.; Zhang, X.; Chen, Y. M. *Int. J. Mod. Phys. B* **1998**, *12*, 3162.

(14) Chen, Y.; Chen, X.; Tang, Z.; Chou, P. C.; Zhang, X.; Ignatiev, A. *Mater. Res. Soc. Symp. Proc.* **2001**, *659*, 334.

(15) Lee, H.-G.; Lee, Y.-M.; Hong, G.-W. *IEEE Trans. Appl. Supercond.* **2001**, *11*, 3333.

(16) McAleese, J.; Darr, J. A.; Steele, B. C. H. *Chem. Vap. Deposition* **1996**, *2*, 244.

(17) Malandrino, G.; Lo Nigro, R.; Benelli, C.; Castelli, F.; Fragalà, I. L. *Chem. Vap. Deposition* **2000**, *6*, 233.

(18) Pan, M.; Meng, G. Y.; Xin, H. W.; Chen, C. S.; Peng, D. K.; Lin, Y. S. *Thin Solid Films* **1998**, *324*, 89.

(19) Daniele, S.; Hubert-Pfalzgraf, L. G.; Perrin, M. *Polyhedron* **2002**, *21*, 1985.

10.1021/cm035392y CCC: $27.50
Published on Web 04/01/2004

Ce(OCMe$_2$-*i*-Pr)$_4$. This complex, which was synthesized first by Bradley et al.,[20] was prepared from $(NH_4)_2Ce(NO_3)_6$ and NaOCMe$_2$-*i*-Pr in THF following a procedure based on the method reported by Gradeff et al.[21,22] as later modified by Evans et al.[23] and Caulton et al.[24] to prepare other Ce(IV) alkoxide derivatives. Ce(OCMe$_2$-*i*-Pr)$_4$ was isolated as a yellow liquid by vacuum distillation (bp 123 °C/10^{-2} Torr; reported bp 132 °C/0.05 Torr)[20] in typically 50−60% yield on a 10-g scale. NMR data have not been reported previously. ^{1}H NMR (C_6D_6): δ 1.04 (d, 6, J = 6.9 Hz, OCMe$_2$CH*Me*$_2$), 1.25 (s, 6, OC*Me*$_2$CHMe$_2$), 1.67 (sept, 1, J = 6.9 Hz, OCMe$_2$C*H*Me$_2$). ^{13}C NMR (C_6D_6): δ 19, 29, 41, 86.

Ce(OCMe$_2$-*i*-Pr)$_4$(DMAP)$_2$. To a solution of Ce(OCMe$_2$-*i*-Pr)$_4$ (0.40 g, 0.73 mmol) in diethyl ether (20 mL) was added 4-(dimethylamino)pyridine (0.18 g, 1.5 mmol). The mixture was stirred for 12 h. The ether was removed in vacuo and the residue was redissolved in hexanes (10 mL). The hexanes solution was filtered through Celite and the filtrate was concentrated in vacuo to about 5 mL. The flask was placed in the freezer overnight whereupon yellow crystals formed (0.42 g, 73%). Anal. Calcd for $C_{38}H_{72}N_4O_4Ce$: C, 57.8; H, 9.20; N, 7.10. Found: C, 57.9; H, 9.32; N, 7.52. ^{1}H NMR (C_6D_6): δ 1.25 (d, 24, J = 6.9 Hz, OCMe$_2$CH*Me*$_2$), 1.55 (s, 24, OC*Me*$_2$CHMe$_2$), 2.06 (sept, 4, J = 6.9 Hz, OCMe$_2$C*H*Me$_2$), 2.12 (s, 12, *Me*$_2$Npy), 6.09 (d, 4, H^{2}and H^6 of Me$_2$Npy), 8.91 (d, 4, H^{3}and H^5 of Me$_2$Npy). ^{13}C{^{1}H} NMR (C_6D_6): δ 19, 29, 38, 42, 84, 106, 151, 154.

Ce$_2$(OCMe$_2$-*i*-Pr)$_5$(acac)$_3$. To a cold (−35 °C) solution of Ce(OCMe$_2$-*i*-Pr)$_4$ (0.40 g, 0.73 mmol) in hexanes (20 mL) was added a solution of acetylacetone (0.11 g, 1.1 mmol) in hexanes (10 mL). The solution momentarily became red, and after the addition was completed, the mixture was pale orange. The mixture was stirred for 12 h. The volatile components were removed in vacuo and the residue was dissolved in a minimum amount of hexanes (1 mL). Orange crystals formed from the solution after storing the flask in the freezer (−35 °C) for several days (0.25 g, 63%). The compound decomposes at room temperature over a period of weeks. Anal. Calcd for $C_{45}H_{86}O_{11}Ce_2$: C, 49.9; H, 8.00. Found: C, 49.4; H, 7.98. ^{1}H NMR (toluene-d_8): δ 1.06 (br m), 1.35 (br s), 1.74 (br s), 2.13 (br s), 5.2 (br s), 5.37 (br s).

X-ray Crystallography. X-ray crystallographic studies were performed on Ce(OCMe$_2$-*i*-Pr)$_4$, Ce(OCMe$_2$-*i*-Pr)$_4$(DMAP)$_2$, and Ce$_2$(OCMe$_2$-*i*-Pr)$_5$(acac)$_3$. Crystals of Ce(OCMe$_2$-*i*-Pr)$_4$ (yellow blocks) were grown from the neat liquid at −35 °C. The crystals were kept cold during the mounting procedure because they melt at just below room temperature. Crystals of Ce(OCMe$_2$-*i*-Pr)$_4$(DMAP)$_2$ (golden blocks) and Ce$_2$(OCMe$_2$-*i*-Pr)$_5$(acac)$_3$ (orange plates) were grown from cold hexanes solutions. In all cases, air-sensitive handling techniques were used during the mounting procedures. Data were collected on a Siemens SMART CCD instrument. Selected details concerning the crystallographic analyses are as follows:

[Ce(OCMe$_2$-*i*-Pr)$_4$]$_2$: $C_{48}H_{104}O_8Ce_2$, fw = 1089.55, crystal dimensions 0.25 × 0.20 × 0.15 mm, triclinic, space group $P\bar{1}$, a = 11.1447(5) Å, b = 14.6246(6) Å, c = 17.5317(8) Å, α = 89.129(1)°, β = 83.068(1)°, γ = 83.560(1)°, T = −50(2) °C, Z = 2, V = 2818.6(2) Å^3, D_{calcd} = 1.284 g/cm^3, μ = 1.637 mm^{-1}, R = 0.0264, R_w = 0.0654. Two of the terminal alkoxide ligands were found to be disordered. The O4/O4′ orientations are present in a 50:50 ratio, while the O5/O5′ orientations are 82:18.

Ce(OCMe$_2$-*i*-Pr)$_4$(DMAP)$_2$: $C_{38}H_{72}CeN_4O_4$, fw = 789.12, crystal dimensions 0.35 × 0.25 × 0.15 mm, monoclinic, space group $C2/c$, a = 39.8617(24) Å, b = 10.5075(6) Å, c = 20.5428(12) Å, β = 95.758(1)°, T = −50(2) °C, Z = 8, V = 8560.9(9) Å^3, D_{calcd} = 1.225 g/cm^3, μ = 1.102 mm^{-1}, R = 0.0298, R_w = 0.0689. One of the alkoxide ligands (O2) was found to be disordered over two different orientations with an approximately 55:45 occupancy.

Ce$_2$(OCMe$_2$-*i*-Pr)$_5$(acac)$_3$: $C_{45}H_{86}Ce_2O_{11}$, fw = 1083.38, crystal dimensions 0.45 × 0.35 × 0.25 mm, monoclinic, space group $P2_1/c$, a = 15.386(2) Å, b = 13.138(1) Å, c = 27.386(3) Å, β = 104.32(1)°, T = −50(2) °C, Z = 4, V = 5363.8(10) Å^3, D_{calcd} = 1.342 g/cm^3, μ = 1.725 mm^{-1}, R = 0.0379, R_w = 0.1024. Four of the alkoxide ligands are disordered. The disorder was treated by a combination of rigid body refinement and distance constraints.

Apparatus for Film Depositions. A horizontal hot wall low-pressure CVD system equipped with mass flow controllers was used for depositions on LAO and nickel substrates. The apparatus is drawn schematically in **I** and is described in detail in a thesis by Mîinea.[25] A simpler version of this apparatus was used for depositions on silicon, glass, and quartz substrates.

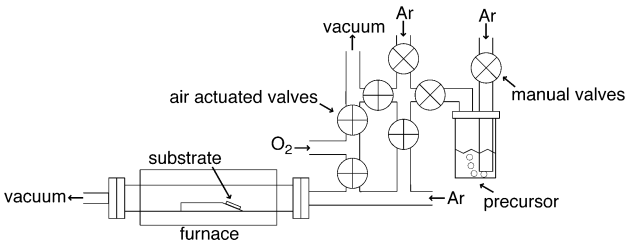

I

Deposition Procedure—Silicon, Glass, and Quartz Substrates. The precursor container was maintained at 84−85 °C. During depositions, three different sections of the precursor feed lines were maintained at temperatures ranging from 95 to 142 °C. The argon (UHP-grade) carrier-gas flow rate through the precursor bubbler was 200 sccm. After passing through the bubbler, the precursor/argon mixture was diluted with more argon (to 800 sccm) before entering the reactor. The typical deposition pressure was 1.0−1.1 Torr. Film depositions were carried out at substrate temperatures in the range 270−530 °C. Silicon substrates (Si (100) or (111)) with dimensions of approximately 1.5 × 2.0 cm were prepared for the film depositions by washing them with hexanes and HF:H_2O (1:10) and then rinsing with distilled water before blow drying with a nitrogen stream. The glass and quartz substrates (1-mm thick) were prepared by washing them with soap, rinsing with distilled water and then methanol, and finally blow-drying with a nitrogen stream.

Deposition Procedure—Lanthanum Aluminum Oxide (LAO) Substrates. The precursor container was maintained at 84−85 °C. During depositions, three different sections of the precursor line were maintained at temperatures ranging from 94 to 114 °C. The argon (UHP-grade) carrier-gas flow rate through the precursor bubbler was 150 sccm. After passing through the bubbler, the precursor/argon mixture was diluted with more argon (to 800 sccm) before being mixed with oxygen (200 sccm) just before entering the reactor. Highly oriented films were grown on LAO (001) at substrate temperatures in the temperature range 500−650 °C. The system pressure during depositions was 2.0−2.5 Torr. The films were annealed under the argon/oxygen flow at the deposition temperature for 1 h after the precursor feed line was turned off. Substrates of LAO (001) with dimensions of approximately 0.5 × 1.0 cm were prepared for the film depositions by washing them in hexanes and acetone using a sonicator and then rinsing with distilled water before drying with a nitrogen stream or in a hot oven.

Deposition Procedure—Textured Nickel Substrates. The precursor container was maintained at 84−85 °C. During

(20) Bradley, D. C.; Chatterjee, A. K.; Wardlaw, W. *J. Chem. Soc.* **1957**, 2600; **1956**, 2260; **1956**, 3469.
(21) Gradeff, P. S.; Schreiber, F. G.; Brooks, K. C.; Sievers, R. E. *Inorg. Chem.* **1985**, *24*, 1110.
(22) Gradeff, P. S.; Schreiber, F. G.; Mauermann, H. *J. Less-Common Met.* **1986**, *126*, 335.
(23) Evans, W. J.; Deming, T. J.; Olofson, J. M.; Ziller, J. W. *Inorg. Chem.* **1989**, *28*, 4027.
(24) Vaartstra, B. A.; Huffman, J. C.; Gradeff, P. S.; Hubert-Pfalzgraf, L. G.; Daran, J.-C.; Parraud, S.; Yunlu, K.; Caulton, K. G. *Inorg. Chem.* **1990**, *29*, 3126.
(25) Mîinea, L. A., Ph.D. Thesis, University of Houston, Houston, TX, 2000.

depositions, three different sections of the precursor line were maintained at temperatures ranging from 94 to 114 °C. The argon (UHP-grade) carrier-gas flow rate through the precursor bubbler was 100 sccm. After passing through the bubbler, the precursor/argon mixture was diluted with more argon (to 800 sccm) before being mixed with oxygen (25 sccm) just before entering the reactor. Depositions were attempted at substrate temperatures in the range 450−900 °C. The films were annealed after deposition at 450−500 °C under an argon/oxygen flow for 1 h. The system pressure during depositions was 2.0−2.5 Torr. The roll-textured Ni (001) substrates were obtained from Professor Kamel Salama at the University of Houston. The substrates were cut from a long ribbon to dimensions of approximately 0.5 × 1.0 cm. The substrates were prepared for the depositions by washing them in hexanes and acetone using a sonicator and then rinsing with distilled water before drying with a nitrogen stream or in a hot oven.

Film Characterization. X-ray diffraction (XRD) powder and thin film studies were performed using Siemens D5000 diffractometers (Cu Kα radiation; 0.01° step size). Siemens general area detector diffraction software (GADDS) was used for film ϕ scans. X-ray photoelectron spectroscopy (XPS) studies were carried out using a Physical Electronics PHI 5700 ESCA system equipped with a 5-keV Ar^+ sputter gun. The electron-energy analyzer was referenced to the Au $4f_{7/2}$ line at 84 eV. XP spectra during depth profile analyses were collected using a standard Al Kα source. The width was set at 11.75 eV throughout. The base pressure was 2×10^{-8} Torr during sputtering. Spectra were collected using a monochromated Al source at a pass energy of 23.5 eV. The base pressure was below 10^{-9} Torr. Scanning electron microscopy (SEM) and electron backscatter diffraction (EBSD) data collection was accomplished using a JEOL JSM-6330F instrument. The film thicknesses used in the growth rate calculations were obtained from SEM cross-sectional views. Transmittance spectra were collected on a Varian Cary 8452A diode array spectrophotometer. Dr. Yongqiang Wang at the Ion Beam Analysis Facility, University of Minnesota, collected the Rutherford backscattering spectrometry (RBS) data. The beam was 2-MeV $^4He^+$, and the total charge collected for the spectrum was 10 μC at 10 nA. The RBS detector (fwhm = 18 keV, Ω = 4.16 msr) was located at 165°. The backscattering data were analyzed locally by using the commercial program RUMP.

Results and Discussion

Synthesis and Characterization. The complex $Ce(OCMe_2\text{-}i\text{-}Pr)_4$ was chosen for use as a precursor to ceria because it was reported to be a liquid, have a low boiling point, and have good thermal stability. Bradley, Chatterjee, and Wardlaw synthesized $Ce(OCMe_2\text{-}i\text{-}Pr)_4$ originally via alkoxide/alcohol exchange using $[Ce(O\text{-}i\text{-}Pr)_4(HO\text{-}i\text{-}Pr)]_2$ as the starting material. We prepared it more conveniently and inexpensively according to eq 1, which is based on the method reported by Gradeff et al.[21,22] as later modified by Evans et al.[23] and Caulton et al.[24] On a multigram scale, the complex was isolated in 50−60% yield after vacuum distillation. It crystallizes as a dimer from the neat liquid (see below) when it is stored in the freezer but the crystals melt at approximately 20 °C.

$$(NH_4)_2Ce(NO_3)_6 + 6NaOCMe_2\text{-}i\text{-}Pr \rightarrow Ce(OCMe_2\text{-}i\text{-}Pr)_4 + 6NaNO_3 + 2NH_3 + 2HOCMe_2\text{-}i\text{-}Pr \quad (1)$$

In related synthetic studies, we synthesized the 4-(dimethylamino)pyridine adduct $Ce(OCMe_2\text{-}i\text{-}Pr)_4(DMAP)_2$ (eq 2) for an X-ray study. In addition, in an attempt to prepare the alkoxide/β-diketonate derivative "$Ce(OCMe_2\text{-}i\text{-}Pr)_3(acac)$" for possible use as an oxide precursor, we reacted $Ce(OCMe_2\text{-}i\text{-}Pr)_4$ with acetylacetone in a 1:1 stoichiometry. Instead of the expected complex, $Ce_2(OCMe_2\text{-}i\text{-}Pr)_5(acac)_3$ was isolated from the reaction mixture as orange crystals in low yield. With adjustment of the reaction stoichiometry (eq 3), $Ce_2(OCMe_2\text{-}i\text{-}Pr)_5(acac)_3$ was subsequently obtained in 63% yield. $Ce_2(OCMe_2\text{-}i\text{-}Pr)_5(acac)_3$ is extremely soluble in hydrocarbons, and it decomposes slowly when stored at room temperature. The latter fact precludes its use as a practical CVD precursor.

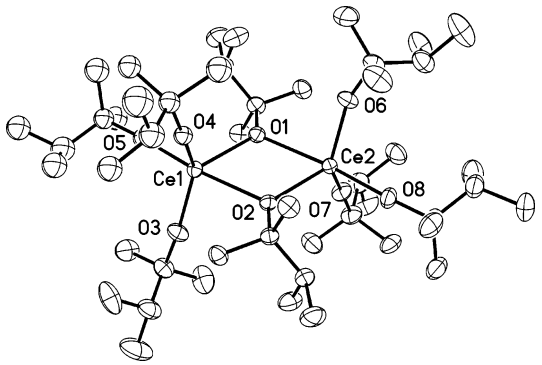

Figure 1. Plot of $[Ce(OCMe_2\text{-}i\text{-}Pr)_4]_2$ showing the atom numbering scheme for the core atoms (40% equiprobability envelopes with hydrogen atoms omitted). Selected bond distances (Å) and angles (deg): Ce1−O1, 2.291(2); Ce1−O2, 2.468(3); Ce2−O1, 2.460(3); Ce2−O2, 2.294(2); avg. $Ce-O_{term}$, 2.085; O1−Ce1−O3, 116.41(10); O1−Ce1−O4, 106.1(2); O3−Ce1−O4, 133.6(2); O2−Ce1−O5, 171.07(15); O2−Ce2−O6, 115.77(10); O2−Ce2−O7, 113.00(10); O6−Ce2−O7, 127.75(11); O1−Ce2−O8, 171.52(9).

$$Ce(OCMe_2\text{-}i\text{-}Pr)_4 + 2DMAP \rightarrow Ce(OCMe_2\text{-}i\text{-}Pr)_4(DMAP)_2 \quad (2)$$

$$2Ce(OCMe_2\text{-}i\text{-}Pr)_4 + 3Hacac \rightarrow Ce_2(OCMe_2\text{-}i\text{-}Pr)_5(acac)_3 + 3HOCMe_2\text{-}i\text{-}Pr \quad (3)$$

X-ray crystallographic studies were performed on $Ce(OCMe_2\text{-}i\text{-}Pr)_4$ (Figure 1), $Ce(OCMe_2\text{-}i\text{-}Pr)_4(DMAP)_2$ (Figure 2), and $Ce_2(OCMe_2\text{-}i\text{-}Pr)_5(acac)_3$ (Figure 3). Selected bond distances and angles are presented in the figure captions.

The complex $Ce(OCMe_2\text{-}i\text{-}Pr)_4$ is dimeric in the solid state with two bridging alkoxide ligands (i.e., the molecule is $[Ce(OCMe_2\text{-}i\text{-}Pr)_3(\mu\text{-}OCMe_2\text{-}i\text{-}Pr)]_2$). The four-member $Ce1(\mu\text{-}OR)_2Ce2$ ring has two long (2.47 Å) and two short Ce−O (2.29 Å) distances, suggesting the former corresponds to RO → Ce dative bonds. The geometry at the five-coordinate cerium atoms can be described as distorted trigonal bipyramidal with a terminal ligand and a bridging ligand (O2−Ce1−O5 and O1−Ce2−O8) occupying the apical positions. Structurally characterized five-coordinate cerium complexes are not common.[26−29] The results of the X-ray analysis are in contrast to solution ebullioscopic data reported by

(26) Morton, C.; Alcock, N. W.; Lees, M. R.; Munslow, I. J.; Sanders, C. J.; Scott, P. *J. Am. Chem. Soc.* **1999**, *121*, 11255.
(27) Cary, D. R.; Arnold, J. *J. Am. Chem. Soc.* **1993**, *115*, 2520.
(28) Cary, D. R.; Ball, G. E.; Arnold, J. *J. Am. Chem. Soc.* **1995**, *117*, 3492.
(29) Lee, L.; Berg, D. J.; Bushnell, G. W. *Inorg. Chem.* **1994**, *33*, 5302.

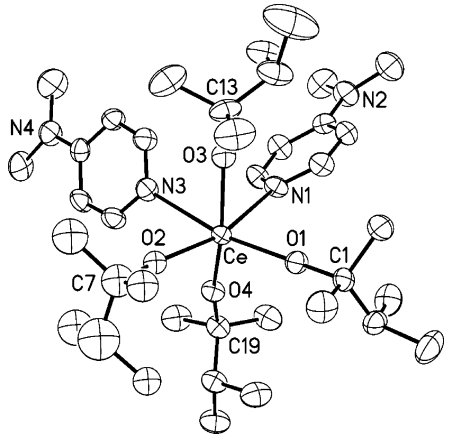

Figure 2. Plot of $[Ce(OCMe_2\text{-}i\text{-}Pr)_4]_2(DMAP)_2$ showing the atom numbering scheme for selected atoms (40% equiprobability envelopes with hydrogen atoms omitted). Selected bond distances (Å) and angles (deg): Ce−O1, 2.112(3); Ce−O2, 2.112(8); Ce−O3, 2.124(3); Ce−O4, 2.129(3); Ce−N1, 2.677(3); Ce−N3, 2.658(3); O1−Ce−O2, 109.3(3); O1−Ce−O3, 95.52(10); O1−Ce−O4, 98.90(10); O1−Ce−N1, 88.03(10); O1−Ce−N3, 166.56(10); O2−Ce−O3, 93.3(3); O2−Ce−O4, 96.7(2); O2−Ce−N1, 162.5(3); O2−Ce−N3, 84.0(3); O3−Ce−O4, 158.61(11); O3−Ce−N1, 82.14(10); O3−Ce−N3, 81.08(11); N1−Ce−O4, 82.65(10); N1−Ce−N3, 78.65(10).

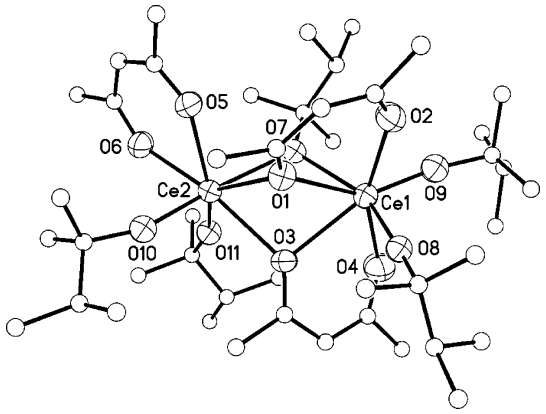

Figure 3. Plot of $Ce_2(OCMe_2\text{-}i\text{-}Pr)_5(acac)_3$ showing the atom numbering scheme for the core atoms (40% equiprobability envelopes with hydrogen atoms omitted). Selected bond distances (Å) and angles (deg): Ce1−O1, 2.508(4); Ce1−O2, 2.357(5); Ce1−O3, 2.494(4); Ce1−O4, 2.424(5); Ce1−O7, 2.367(4); Ce1−O8, 2.054(7); Ce1−O9, 1.960(13); Ce2−O1, 2.689(4); Ce2−O3, 2.475(4); Ce2−O5, 2.355(4); Ce2−O6, 2.370(4); Ce2−O7, 2.361(4); Ce2−O10, 2.033(6); Ce2−O11, 2.095(6); O7−Ce1−O8, 153.0(3); O7−Ce2−O10, 165.2(3); $\Sigma[Om\text{−}Ce1\text{−}On]_{cis}$ ($m \neq n = 1, 2, 3, 4, 9$), 361; $\Sigma[Om\text{−}Ce2\text{−}On]_{cis}$ ($m \neq n = 1, 3, 5, 6, 11$), 360.

Bradley et al., which indicated that $Ce(OCMe_2\text{-}i\text{-}Pr)_4$ is monomeric in benzene and toluene solutions.[20]

Six-coordinate $Ce(OCMe_2\text{-}i\text{-}Pr)_4(DMAP)_2$ (Figure 2) can be described as having a highly distorted octahedral geometry. The structure closely resembles $Ce[OCH(CF_3)_2]_4(TMEDA)$ and $Ce(OSiPh_3)_4(DME)$,[19,30] the latter described by Gradeff et al. as a bicapped tetrahedron.

The molecule $Ce_2(OCMe_2\text{-}i\text{-}Pr)_5(acac)_3$ (Figure 3) has two terminal alkoxide ligands at each cerium atom (O8−O11). The cerium atoms are linked by one bridging alkoxide ligand (O7) and two acac ligands that each bridges the cerium atoms through one oxygen atom (O1 and O3). The other two oxygen atoms of the bridging acac ligands (O2 and O4) are terminally bound to Ce1. Another acac ligand is terminally bonded to Ce2. Thus, each cerium atom is bonded to seven oxygen atoms. As emphasized in diagram **II**, the seven-coordinate cerium atoms have distorted pentagonal bipyramidal coordination geometries.

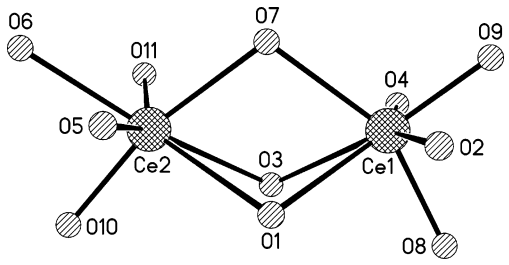

II

The $Ce\text{−}OR_{term}$ distances in $[Ce(OCMe_2\text{-}i\text{-}Pr)_4]_2$, $Ce(OCMe_2\text{-}i\text{-}Pr)_4(DMAP)_2$, and $Ce_2(OCMe_2\text{-}i\text{-}Pr)_5(acac)_3$ fall near the range of distances reported for $Ce(O\text{-}t\text{-}Bu)_2(NO_3)_2(HO\text{-}t\text{-}Bu)_2$ (2.026(5) and 2.023(5) Å),[23] $[Ce(O\text{-}i\text{-}Pr)_3(HO\text{-}i\text{-}Pr)(\mu\text{-}O\text{-}i\text{-}Pr)]_2$ (2.083(6) and 2.093(6) Å),[24] and $Ce[OCH(CF_3)_2]_4L_2$ (L_2 = TMEDA or diglyme) (2.115(4)−2.139(5) Å).[19] The $Ce\text{−}OR_{bridge}$ distances in $Ce_2(OCMe_2\text{-}i\text{-}Pr)_5(acac)_3$ are close to those in $[Ce(O\text{-}i\text{-}Pr)_3(HO\text{-}i\text{-}Pr)(\mu\text{-}O\text{-}i\text{-}Pr)]_2$ (2.325(6) and 2.338(6) Å).[24] Two of the bridging distances in $[Ce(OCMe_2\text{-}i\text{-}Pr)_4]_2$ are much shorter and two are much longer than those in $[Ce(O\text{-}i\text{-}Pr)_3(HO\text{-}i\text{-}Pr)(\mu\text{-}O\text{-}i\text{-}Pr)]_2$ and $Ce_2(OCMe_2\text{-}i\text{-}Pr)_5(acac)_3$, reflecting the loose association of the $Ce(OCMe_2\text{-}i\text{-}Pr)_4$ units in the dimer. The Ce−N distances in $Ce(OCMe_2\text{-}i\text{-}Pr)_4(DMAP)_2$ are very close to the one reported for triindenylcerium pyridinate (2.684(4) Å).

Room-temperature NMR spectra for $Ce(OCMe_2\text{-}i\text{-}Pr)_4$, $Ce(OCMe_2\text{-}i\text{-}Pr)_4(DMAP)_2$, and $Ce_2(OCMe_2\text{-}i\text{-}Pr)_5(acac)_3$ indicate that all three undergo fluxional processes. Spectra for $Ce(OCMe_2\text{-}i\text{-}Pr)_4$ and $Ce(OCMe_2\text{-}i\text{-}Pr)_4(DMAP)_2$ collected at −70 and −35 °C, respectively, were not significantly different from the room-temperature spectra. Low-temperature ^1H NMR spectra for $Ce_2(OCMe_2\text{-}i\text{-}Pr)_5(acac)_3$, however, showed sharpening of the resonances as the probe was cooled. At −70 °C, the MeC(O)C*H*C(O)Me region of the spectra consistently showed three sharp peaks of equal intensity at δ 5.46, 5.42, and 5.34 together with two peaks in a 2:1 integral ratio at δ 5.30 and 5.10. The total intensity of the latter two peaks relative to the first three varied with the concentration of the sample. Tentatively, the spectra are interpreted as being the result of an equilibrium involving $Ce_2(OR)_5(acac)_3$ and the two monomers $Ce(OCMe_2\text{-}i\text{-}Pr)_2(acac)_2$ and $Ce(OCMe_2\text{-}i\text{-}Pr)_3(acac)$. The three peaks of equal intensity are assigned to the parent dimer, $Ce_2(OCMe_2\text{-}i\text{-}Pr)_5(acac)_3$, and the other two peaks to $Ce(OCMe_2\text{-}i\text{-}Pr)_2(acac)_2$ and $Ce(OCMe_2\text{-}i\text{-}Pr)_3(acac)$.

Film Depositions on Silicon, Glass, and Quartz. Low-pressure CVD using $Ce(OCMe_2\text{-}i\text{-}Pr)_4$ as a single-source precursor gave shiny films at substrate temperatures of 330−530 °C but no films were formed at 270 °C. When O_2 was used as a co-precursor, however, a film formed at 270 °C but none were deposited at ≈230 °C. Film compositions and growth rates, which were calculated from film thickness data obtained by SEM, are presented in Table 1.

(30) Gradeff, P. S.; Yunlu, K.; Gleizes, A.; Galy, J. *Polyhedron* **1989**, *8*, 1001.

Table 1. Compositions and Growth Rates for Films Deposited on Silicon from $Ce(OCMe_2$-*i*-$Pr)_4$

deposition temp (°C)	O/Ce[a]	growth rate[b] (Å/min)
270[c]	2.2	110
330	2.2	95
400	2.2	131
460	2.2	142
530	2.2	145

[a] From RBS spectra. The error is estimated to be ±0.1. [b] Film thickness obtained by cross-sectional SEM. The error is estimated to be ±5%. [c] Deposition performed with oxygen.

X-ray photoelectron spectra for as-deposited films (i.e., not sputtered) on silicon at 270 and 400 °C showed the features characteristic of CeO_2.[3,33−38] For the film deposited at 400 °C, the cerium 3d region consisted of three $3d_{5/2}$ peaks at 882.75, 889.19, and 898.78 eV and three $3d_{3/2}$ peaks at 901.36, 907.8, and 917.39 eV. The spectra for the film deposited at 270 °C was similar. In their early work, Burroughs et al.[38] referred to these series of peaks as v, v′′, v′′′ and u, u′′, u′′′, respectively, the notation adopted by other authors in later studies. The features referred to as v′ (~885 eV) and u′ (~904 eV) by Burroughs et al., which recent theoretical and experimental studies ascribe to Ce_2O_3 impurities,[33,35] were absent in our spectra. The 3d multiplet splitting (u−v, u′′′−v′′′) of 18.6 eV, and the u−u′′′ and v−v′′′ separation of 16.0 eV, were in good agreement with the corresponding values reported in the literature for CeO_2 (18.7 and 15.8 eV, respectively).[38,39]

To better analyze the composition, attempts were made to sputter the film deposited at 400 °C with 1- and 5-keV Ar^+ but this resulted in a massive reduction of the CeO_2 to Ce_2O_3 due to the differential yield of oxygen atoms in the sputtering process. With use of a low-energy sputter ion (500-eV Ar^+) and a long sputtering time (50 min), however, a spectrum was obtained that showed no significant reduction and gave an O/Ce ratio of 1.99. A small amount of carbon was also present (approximately 3%). These results are in agreement with the studies made by Paparazzo et al.,[32,33] Allen,[40] and Holgado et al.[36] on the damage induced by X-rays and Ar^+ sputtering on CeO_2.

Given the difficulties that may arise in the analysis of cerium oxide by XPS, we turned to RBS and XRD for further characterization. Rutherford backscattering spectrometry spectra for films deposited at 270 (with O_2), 330, 400, 460, and 530 °C on silicon (e.g., Figure 4) indicated that each had stoichiometries close to CeO_2. Carbon peaks were not observed in any of the spectra, indicating low carbon contamination levels (<5 atom %). This is consistent with the XPS results.

(31) Zazzetta, A.; Greco, A. *Acta Crystallogr.* **1979**, *B35*, 457.
(32) Paparazzo, E.; Ingo, G. M.; Zacchetti, N. *J. Vac. Sci. Technol. A* **1991**, *9*, 1416.
(33) Paparazzo, E. *Surf. Sci.* **1990**, *234*, L253 and references therein.
(34) Paparazzo, E. *J. Vac. Sci. Technol. B* **2000**, *18*, 296.
(35) Le Normand, F.; El Fallah, J.; Hilaire, L.; Légaré, P.; Kotani, A.; Parlebas, J. C. *Solid State Commun.* **1989**, *71*, 885.
(36) Holgado, J. P.; Alvarez, R.; Munuera, G. *Appl. Surf. Sci.* **2000**, *161*, 301.
(37) Ingo, G. M.; Papparazo, E.; Bagnarelli, O.; Zachetti, N. *Surf. Interface Anal.* **1990**, *16*, 515.
(38) Burroughs, P.; Hamnett, A.; Orchard, F. A.; Thornton, G. *J. Chem. Soc., Dalton Trans.* **1976**, 1686.
(39) Kaindl, G.; Wertheim, G. K.; Schmiester, G.; Sampathkumaran, E. V. *Phys. Rev. Lett.* **1987**, *58*, 606.
(40) Allen, J. W. *J. Magn. Magn. Mater.* **1985**, *47 & 48*, 168.

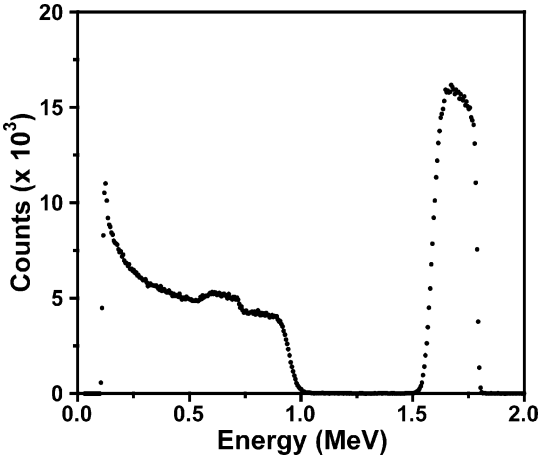

Figure 4. Rutherford backscattering spectrum of a cerium oxide film deposited at 400 °C on silicon. The thickness is about 5000 Å.

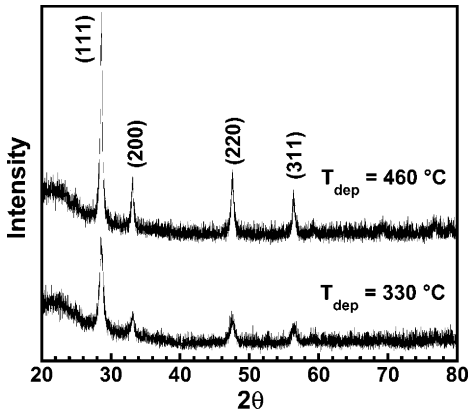

Figure 5. X-ray diffraction patterns for as-deposited cerium oxide films deposited at 330 and 460 °C.

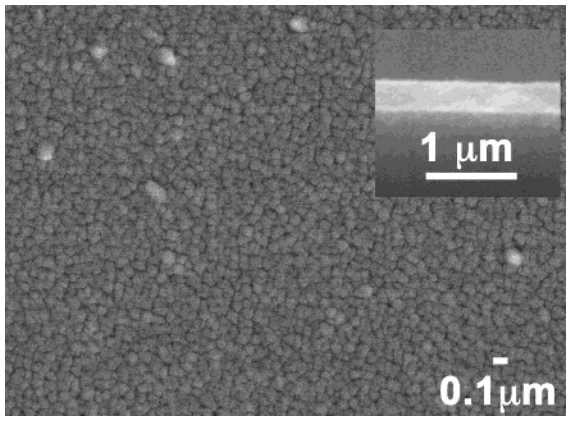

Figure 6. SEM of a cerium oxide film deposited at 400 °C. The inset shows a side-on view of the same film.

X-ray diffraction patterns for 3200- and 4500-Å films deposited at 330 and 460 °C, respectively, on quartz are shown in Figure 5. The broad diffraction peaks are consistent with CeO_2. Scanning electron micrographs for the films deposited on Si (100) indicated that the film surfaces had similar grain structures independent of the deposition temperature. The scanning electron micrograph for the film deposited at 400 °C is shown in Figure 6. Transmission spectra for 3800−5600-Å films grown on quartz at 270, 330, 400, and 460 °C are shown in Figure 7. The absorption edges did not vary appreciably with the deposition temperature.

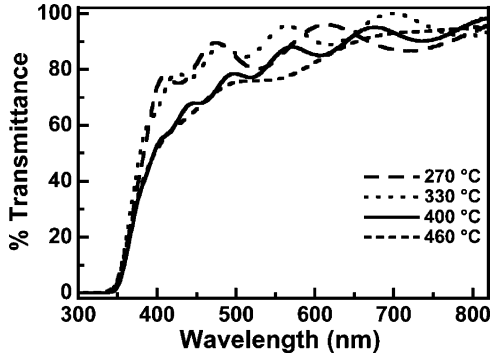

Figure 7. UV−vis transmission spectra for cerium oxide films grown on quartz substrates at 270, 330, 400, and 460 °C.

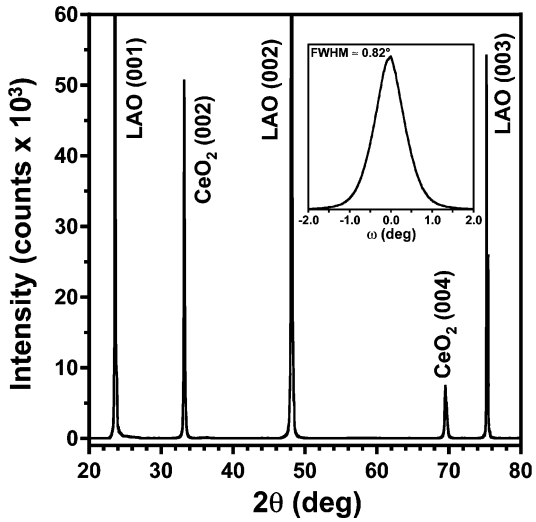

Figure 8. XRD $\theta-2\theta$ pattern and (002) reflection rocking curve (inset) for a cerium oxide film deposited at 550 °C on LAO (001).

Film Depositions on LAO and Ni Substrates. Attempts to grow oriented films on LAO (001) and roll-textured Ni (001) substrates using $Ce(OCMe_2\text{-}i\text{-}Pr)_4$ under conditions similar to those employed for silicon, glass, and quartz substrates failed to give consistently high quality films. The films were either amorphous or poorly crystalline with random orientation. For this reason, we modified the film preparation conditions to include using oxygen as a co-reactant and heating the film after deposition under an oxygen flow.

On LAO (001) substrates, high-quality films were consistently grown by depositing the films at 550 °C using a 20% O_2 flow followed by an annealing cycle at 550 °C for 1 h under the 20% O_2 flow. As an example, the XRD $\theta-2\theta$ pattern and (002) reflection rocking curve for a 4500-Å film (determined by a cross-sectional SEM view) deposited rapidly at approximately 850 Å/min is shown in Figure 8. The pattern indicates the film has only an out-of-plane (001) orientation on the (001) single-crystal substrate. The full-width at half-maximum (fwhm) from the ω-scan rocking curve for the (002) reflection is 0.82°, which is close to the value of 0.85° reported by Marks et al. for CeO_2 grown on YSZ (001) at 540 °C.[2] The fwhm value shows that the film growth plane is aligned with respect to the substrate surface. For the same film, a scanning electron micrograph shows it has a smooth, crack-free surface despite the rapid growth rate. An XRD ϕ-scan at CeO_2 (111) (Figure 9) indicates the film has good in-plane order with respect to the LAO substrate with the fwhm ≈ 2°.

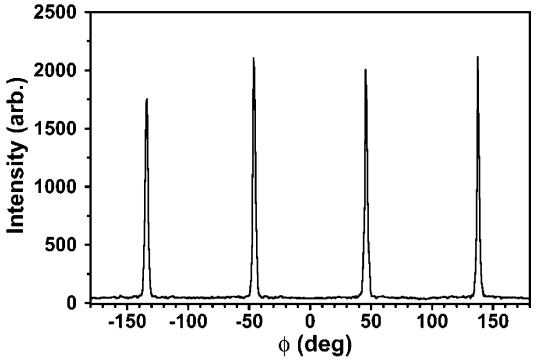

Figure 9. XRD ϕ-scan at CeO_2(111) for a cerium oxide film deposited at 550 °C on LAO (001).

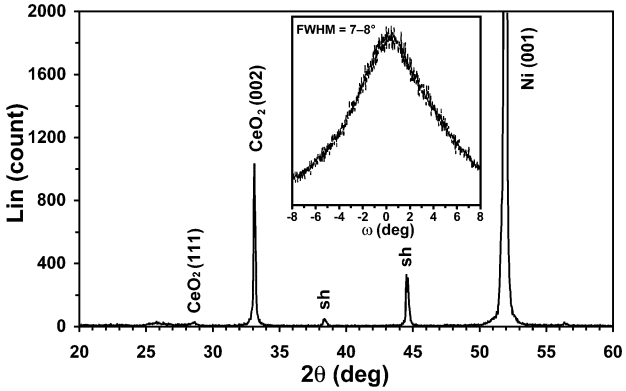

Figure 10. XRD $\theta-2\theta$ pattern and (002) reflection rocking curve (inset) for a cerium oxide film deposited at 500 °C on a roll-textured nickel (001) substrate (peaks labeled "sh" are from the sample holder).

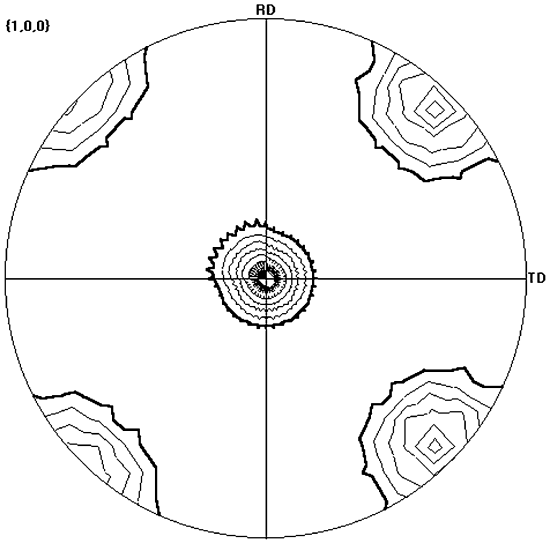

Figure 11. Electron backscatter diffraction pattern for the film deposited at 500 °C on a roll-textured nickel (001) substrate.

Different deposition and annealing conditions were employed when roll-textured Ni (001) was the substrate. On this substrate, high-quality films were consistently deposited at 500 °C using a 3% O_2 flow followed by an annealing cycle at 470 °C for 1 h under the 3% O_2 flow. The lower oxygen flow and annealing temperature was necessary to avoid the formation of NiO (as indicated by XRD analysis). The XRD $\theta-2\theta$ pattern and (002)

reflection rocking curve for a film deposited under these conditions are shown in Figure 10. They show the film has an out-of-plane (001) orientation and a ω-scan fwhm of 7−8°, which is close to the fwhm of 6.2° found for the Ni substrate. To judge in-plane order for the same film, an electron backscatter diffraction pattern was collected (Figure 11), which showed good in-plane ordering.

Conclusion

This study shows that nonfluorinated cerium(IV) alkoxide complexes are viable CVD precursors to cerium oxide. The alkoxide complexes are particular attractive precursors for future studies and applications because of the ease at which their properties (e.g., boiling point and thermal stability) can be tuned by changing the alkoxide-ligand substituent. In the present case, the inexpensive and easily synthesized derivative $Ce(OCMe_2\text{-}i\text{-}Pr)_4$ produced cerium(IV) oxide films rapidly in a conventional thermal CVD process at low substrate temperatures (<550 °C). Importantly, the new precursor system deposited highly oriented cerium oxide on single-crystal LAO (001) and roll-textured nickel (001) substrates. The successful deposition on textured nickel opens the possibility of using these cerium oxide films as buffer layers in YBCO-based coated conductor applications. Further studies to demonstrate the practicality of using the films for this application are needed.

Acknowledgment. Dr. James Korp provided technical assistance with the crystal structure determinations. The Robert A. Welch Foundation and the U.S. Air Force Office of Scientific Research supported this research.

Supporting Information Available: Three complete X-ray crystallographic files in CIF format. This material is available free of charge via the Internet at http://pubs.acs.org.

CM035392Y